Microchimica Acta (2019) 186:495
https://doi.org/10.1007/s00604-019-3619-y

ORIGINAL PAPER

Impedimetric aptasensing of the breast cancer biomarker HER2 using a glassy carbon electrode modified with gold nanoparticles in a composite consisting of electrochemically reduced graphene oxide and single-walled carbon nanotubes

Parvin Forootan Rostamabadi[1] · Esmaeil Heydari-Bafrooei[1]

Received: 12 March 2019 / Accepted: 15 June 2019

Abstract

A method is presented for electrochemical determination of the breast cancer biomarker HER2. A glassy carbon electrode (GCE) was modified with densely packed gold nanoparticles placed on a composite consisting of electrochemically reduced graphene oxide and single walled carbon nanotubes (ErGO-SWCNTs). An aptamer directed against HER2 was then immobilized ono the GCE. The modified GCE was characterized by cyclic voltammetry, differential pulse voltammetry and electrochemical impedance spectroscopy. The immobilized aptamer selectively recognizes HER2 on the electrode interface, and this leads to an increased charge transfer resistance (R_{ct}) of the electrode when using ferri/ferro-cyanide as the electrochemical probe. The method has a low limit of detection (50 fg·mL^{-1}) and a wide analytical range (0.1 pg·mL^{-1} to 1 ng·mL^{-1}). The assay is highly reproducible and specific. Clinical application was demonstrated by analysis of the HER2 levels in serum samples, and sera of breast cancer patients were successfully discriminated from sera of healthy persons.

Keywords DNA aptamer · Electrochemical impedance spectroscopy · Voltammetry · Biosensor

Introduction

Human epidermal growth factor receptor 2 (HER2) levels is clinically used as an indicator of the breast cancer screening [1]. Research has shown that the concentration of HER2 in the blood of healthy people is on average about 2–15 ng·mL^{-1} and increases in breast cancer patients by 15–75 ng·mL^{-1} [2]. Therefore, development of fast and low-cost analytical methods for accurate HER2 detection is of great importance in the early cancer diagnosis, monitoring the effectiveness of treatment and assessing likelihood of remission post treatment.

Currently, the only techniques that have been U.S. Food and Drug Administration (FDA) approved for HER2 status detection involve DNA (in-situ hybridization, ISH) and protein (immunohistochemistry, IHC) evaluation [3, 4]. These techniques, however, are expensive, time consuming, limited sensitivity and specify, and very invasive [5, 6]. Therefore, the development of a costly-effective, fast, facile, sensitive, selective and non-invasive method for the HER2 detection is required. For this purpose, a range of assays have been reported, including fluorescence, chromatography, mass spectroscopy and electrochemistry [7–13]. By comparison, electrochemical (bio)sensors are most appropriate because of their relative simplicity in terms of instrumentation and analysis, low cost per assay, high selectivity and superior sensitivity, reliability, quick response and potential for miniaturization [14–18].

Aptamers are single-stranded sequences that can bind specifically to the target molecules (e.g., proteins and drugs), that can be considered oligonucleotide analogs of antibodies as biorecognition layer in biosensors. Aptamers have numerous advantages over antigene-antibody such as they can be selected by in vitro technologies for their target molecules and they are thermally stable under high temperatures, and they are greatly flexible and easily modifiable with functional groups. Therefore, the use of aptamers as receptor in electrochemical

Electronic supplementary material The online version of this article (https://doi.org/10.1007/s00604-019-3619-y) contains supplementary material, which is available to authorized users.

✉ Esmaeil Heydari-Bafrooei
heydari1983@gmail.com; e.heydari@vru.ac.ir

[1] Department of Chemistry, Faculty of Science, Vali-e-Asr University of Rafsanjan, Rafsanjan 77188–97111, Iran

Published online: 03 July 2019

biosensors has increased sharply [19–21]. Nanomaterials can be used as substrate for immobilization of aptamer, or as labels to amplify electrochemical current. Both factors improve detection limits. Carbon nanomaterials, including single- and multi-walled carbon nanotubes, nanodiamonds, fullerene, nanoporous carbon, carbon dots and graphene oxides are reported in the field of electrochemical biosensing devices [22, 23]. Among them, the most extensively used carbonaceous nanomaterials utilized in electrochemical biosensors are carbon nanotubes and various kinds of graphene [19, 20, 24, 25]. The great mechanical flexibility, high surface-to-volume ratio, high efficiency of charge transfer, the abundant presence of edge-plane-like defects, exceptional electronic properties, unique electrochemical stability and excellent thermal conductivity, allow being used as very attractive materials for the construction of electrochemical (bio)sensors. Their high surfaces of carbon nanotubes can be readily modified with a diversity of functional chemical groups for bioreceptor immobilization that it is gaining importance in the construction of electrochemical biosensors. Nanocomposites prepared by a combination of carbon nanotubes and other materials, such as metal nanoparticles, polymers or ionic liquids are used to improve the electrocatalytic properties and better immobilization of biorecognition elements [26, 27].

In the current study, considering benefits of graphene oxide, AuNPs, and SWCNT nanomaterials, we used them into an aptamer-based assay to apply the synergy contributions on the enhancement of signal characteristics. Anti-HER2 aptamer containing a sequence of 86 bases [28] was used in conjugation with electrochemical impedance spectroscopy (EIS) to monitor HER2 concentration. Furthermore, the electrochemical assay was used for real sample analysis in order to determine HER2 concentration in serum samples obtained from patients with breast cancer.

Experimental section

Chemicals and instrumentation

Anti-HER2 DNA aptamer (APT): 5'-SH-$(CH_2)_6$-AAC CGC CCA AAT CCC TAA GAG TCT GCA CTT GTC ATT TTG TAT ATG TAT TTG GTT TTT GGC TCT CAC AGA CAC ACT ACA CAC GCA CA −3′ was purchased from Bioneer Corporation (www.bioneer.com, Daejeon, Korea). Graphite as a source of graphene oxide (GO), chicken egg white lysozyme, prostate-specific antigen (PSA), thrombin and HER2 were obtained from Sigma-Aldrich (www.sigmaaldrich.com, St. Louis, MO). Aptamer and HER2 solutions were prepared using Tris buffer (containing 10 mmol·L^{-1} Tris–HCl, 1.0 mmol·L^{-1} EDTA and 10 mmol·L^{-1} NaCl, pH 7.4) and were stored at −4 °C until use. The redox probe (3.0 mmol·L^{-1} of $[Fe(CN)_6]^{3-/4-}$ (1:1) mixture and 0.1 mol·L^{-1} KCl in Tris buffer) was prepared immediately before use. In addition, double distilled water was used for the preparation of all aqueous solutions. All reagents were obtained in analytical and extra pure grade and used without any additional purification.

An Autolab PGSTAT302N (www.metrohm-autolab.com) with NOVA 1.11 software (Eco Chemie, The Netherlands, www.ecochemie.nl) in a three electrode cell assembly was used for electrochemical measurements. Field emission-scanning electron microscopy (FE-SEM; Model XL30, Philips) and transmission electron microscopy (TEM) were used for the surface morphology analysis (with a Philips CM30 300 kV TEM operating at 300 kV). UV-Vis absorption spectrum was conducted by a double beam (Jasco V–570 Model) UV-Vis-NIR spectrophotometer with a 1.0 cm quartz cell. Fourier Transform Infrared (FT-IR) spectra were recorded in KBr pellets with a Jasco 680-plus spectrometer from 4000 to 400 cm^{-1}. A Bruker D8/Advance X-ray diffractometer device (using Cu-Ka radiation) was used for preparing the X-ray diffraction (XRD) pattern. Raman spectra were measured using Nicolet Almega® device.

Synthesis of GO-SWCNT

Functionalization of SWCNT to carboxylated SWCNT (SWCNT-COOH) and synthesis of GO was discussed in the supplementary materials. For the preparation of GO-SWCNT, 10 mg SWCNT and 10 mL of GO (1 mg·mL^{-1}) were mixed and ultrasonicated for 1 h. Finally, the composite was collected and re-dispersed in D.I. water (1 mg·mL^{-1}) after being washed with D.I. water and ethanol for three times and dried.

Immobilization of ErGO-SWCNT and AuNPs on the electrode surface

Glassy carbon electrode (GCE, 3.0 mm diameter, Metrohm) was first polished with Al_2O_3 powder (Aldrich, 0.1, 0.05 mm) using Metrohm polishing kit, and rinsed with deionized water, followed by sonication in ethanol and deionized water. Finally, the GCE were dried under a continuous nitrogen stream at the room temperature. 2.5 μL GO-SWCNT was directly drop cast on the cleaned GCE and allowed to dry. The GO-SWCNT modified electrode was then subjected to a constant potential of −0.9 V (vs. Ag/AgCl) for 1000 s in a phosphate buffer (0.1 mol·L^{-1}, pH 4.2) aqueous solution for the electrochemical reduction of GO to ErGO. The electrochemical deposition of AuNPs were prepared by applying a constant potential of −0.2 V in an electrochemical cell containing 1.0 mmol·L^{-1} $HAuCl_4$ solution containing 0.1 mol·L^{-1} KNO_3 as electrolyte for 180 s. The ErGO-SWCNT/AuNPs films were rinsed with water and dried.

Aptamer covalent immobilization onto ErGO-SWCNT/AuNPs

In order to immobilize the aptamer on the surface of the electrode, the modified GCE electrode was immersed in Tris buffer containing thiolated anti-HER2 aptamer (200 nmol·L^{-1}) for an immersion time of 9 h and then the film was rinsed with Tris buffer (0.1 mol·L^{-1}, pH 7.4). The aptamer modified electrode was further treated with 1.0 mmol·L^{-1} 6-mercapto-1-hexanol for 30 min to obtain a well aligned aptamer monolayer and to deactivate the activated sites of the nanoprobe and prevent their unspecific adsorption. In order to remove aptamer molecules which were not stabilized through covalent bounds, electrodes were washed with Tris buffer a few times.

HER2 detection

After preparing the GCE/ErGO-SWCNT/AuNP/APT, the modified electrode was immersed in Tris buffer containing HER2 with different concentrations for 40 min. Then, the electrodes were rinsed with Tris buffer (pH = 7.4) to remove non-bonded HER2 and finally, electrochemical signals of the electrodes before and after interaction with HER2 were detected using EIS. The changes in the electrochemical signals correlated to its concentration.

Electrochemical measurements

All electrochemical studies were carried out using PG electrode as the working electrode, a Pt counter electrode and Ag/AgCl reference electrode. The electrolyte used in all studies was 3.0 mmol·L^{-1} $[Fe(CN)_6]^{3-}$/$[Fe(CN)_6]^{4-}$ (1:1) solution as a redox probe and 0.1 mol·L^{-1} KCl in Tris buffer (pH 7.4). The electrochemical impedance of the electrodes was measured in a frequency range of 100 mHz to 100 KHz at potential of +0.23 V versus Ag/AgCl with a sinusoidal signal of 10 mV.

Preparation of serum samples

Serum samples of breast cancer patients and healthy persons were acquired from Alzahra Hospital, Isfahan, Iran, and centrifuged with G value of 9990 g before storage in the refrigerator at −20 °C. The supernatant was diluted with Tris buffer before use.

Results and discussion

Characterization of the graphene oxide (GO) nanosheets

Raman spectroscopy, FT-IR, SEM, and XRD techniques were used to determine the characteristics of GO nanosheets. All results indicated the successful synthesis of GO. The results obtained from each technique along with necessary details are presented in "Supplementary Materials" (Section S2.1).

Characterization of GO-SWCNT and ErGO-SWCNT/AuNP

The SEM and TEM images of the SWCNTs, GO, ErGO-SWCNT and ErGO-SWCNT/AuNP is presented in Fig. 1. The SEM and TEM of SWCNT (Fig. 1a and b) shows a tube-like homogeneous structure with rough surface features that dispersed in DMF homogeneously with good dispersion. As shown in Fig. 1c and d, the image of GO shows a sheet and wrinkled structure. The SEM image of ErGO-SWCNT is displayed in images of E and F. The gray lamellar structure is related to the ErGO, which was entirely hidden by SWCNT.

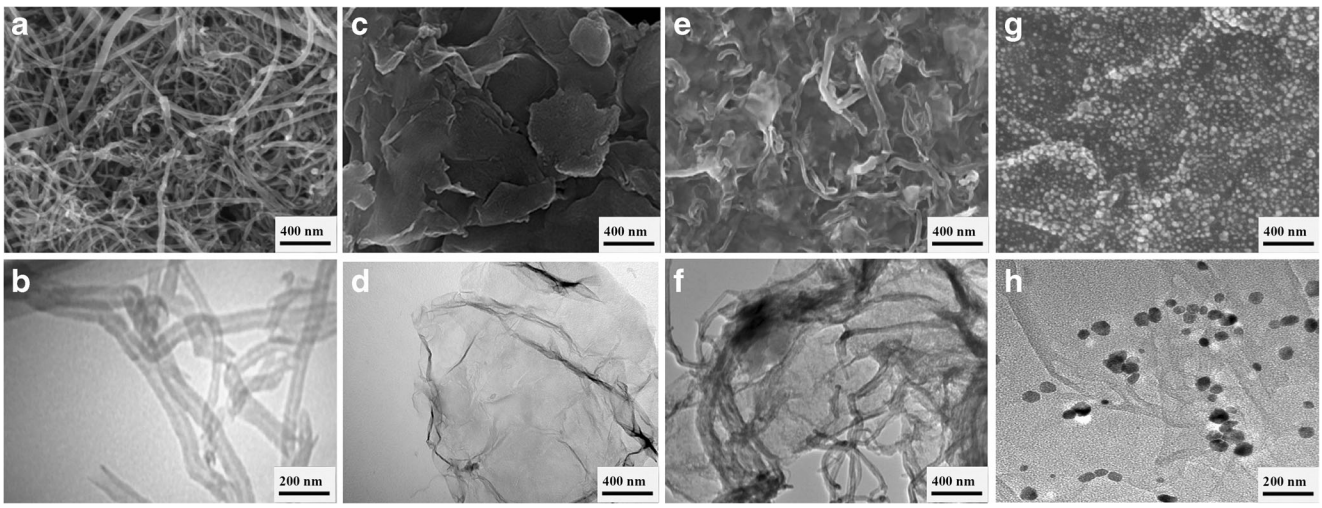

Fig. 1 FE-SEM and TEM images of treated SWCNT (**a** and **b**), GO (**c** and **d**), rGO-SWCNT (**e** and **f**), and rGO-SWCNT/AuNP (**g** and **h**)

CNT not only modified surface properties of the ErGO and avoided from its probable agglomeration, but also exploit as a connection between ErGO and the target molecules. Assemble of the ErGO nanosheets and SWCNT into a nanocomposite lead to producing a new chemical network with favorite structures and attractive properties with both the interesting properties of SWCNT and GO nanosheets. As shown in images of G and H, the AuNP were homogeneously and densely covered on ErGO-SWCNT film. The diameter of AuNP was in a variety of 10–100 nm and the number was excessive. The very minor size and homogeneous and dense spreading of AuNP afforded more opportunity for improving the catalytic activity of ErGO-SWCNT/AuNP film. Generally, the morphology and microstructure characterizations supported the successful creating the ErGO-SWCNT/AuNP nanohybrid with this approach.

The effectiveness of electrochemical reduction of the GO-SWCNT to ErGO-SWCNT was studied by X-ray photoelectron spectroscopy (XPS). Core C1s XPS spectra (Fig. S-2) displays an intense decrease of the C-O bond for ErGO-SWCNT (Fig. S-2B) when compared to GO-SWCNT precursor (Fig. S-2A), likely related to the reduction of epoxides on GO surfaces. It is interesting to investigate the C1s XPS spectrum of rGO after applying potential of −0.2 V to rGO modified GCE (rGO/GCE). As shown in the Fig. S-2C, the XPS spectrum is similar to that of rGO (before applying potential, Fig. S-2B) and not to that of GO (Fig. S-2A). Therefore, the surface oxygen functional groups is not formed on the surface of rGO by applying −0.2 V.

The UV–Vis absorption spectra of the ErGO-SWCNT and ErGO-SWCNT/AuNP nanocomposites are shown in Fig. S-2D. The ErGO-SWCNT displayed an clear characteristic absorption peak at ~228 nm (curve a), which was corresponding to π–π* electronic transitions of aromatic C=C bonds [29]. However, the characteristic absorption peak of aromatic C=C bonds for the ErGO-SWCNT/AuNP nanocomposite was red-shifted to ~245 nm (curve b), indicating that the ErGO-SWCNT was partially reduced by electrochemical treatment [29]. The characteristic absorption peak at ~529 nm on the ErGO-SWCNT/AuNP nanocomposites was attributed to a distinct surface plasmon absorption band of AuNP [30], indicating the growth of AuNP on the surface of ErGO-SWCNT.

The composition and purity of the ErGO-SWCNT/AuNP hybrid nanocomposite were investigated using energy dispersive spectroscopy (EDS) technique as shown in Fig. S-2E. The EDS spectrum shows the well-defined peaks of C and Au without any detectable impurity element, which suggests that the nanocomposite has a high purity in composition. Furthermore, the Raman spectra of the ErGO-SWCNT and ErGO-SWCNT/AuNP nanohybrids were compared in Fig. S-2F. It is clear that the G and D peak positions in the ErGO-SWCNT/AuNP nanohybrid were analogous to those seen in the ErGO-SWCNT, while the ErGO-SWCNT/AuNP nanohybrid had an boosted D/G intensity ratio (ID/IG) of 0.93 (curve b) relative to the GO-SWCNT of 0.80 (curve a), which verified the ErGO-SWCNT has been partially reduced through the electrochemical deposition of AuNP. All the inspections above support the effective production of ErGO-SWCNT/AuNP film.

Investigating the electrochemical properties of the nanocomposites

The electrochemical properties of bare GCE and GO, ErGO, SWCNT, AuNP, ErGO/AuNP, SWCNT/AuNP, and ErGO-SWCNT/AuNP modified GCE were investigated using CV, DPV, and EIS. Figure 2a shows DPV graphs of GCEs modified with different nanomaterials at a solution containing 3.0 mmol·L^{-1} $[Fe(CN)_6]^{3-}$/$[Fe(CN)_6]^{4-}$ (1:1). The graph for the bare GCE (trace a) shows a discrete peak which after coating the GO nanosheet on it shows a sharp decrease in peak current (trace b). This is due to presence of functional groups in GO that hampering electron transfer between the electrode surface and electrolyte, thus reducing the electrical conductivity of GO. After coating GCE with ErGO nanosheet, the current response increases (trace c), while ErGO/AuNP can enhance the electron transfer and available surface of GCE (trace f), leading to an increase in the current response compared to GO. This is the result of high conductivity, large surface area

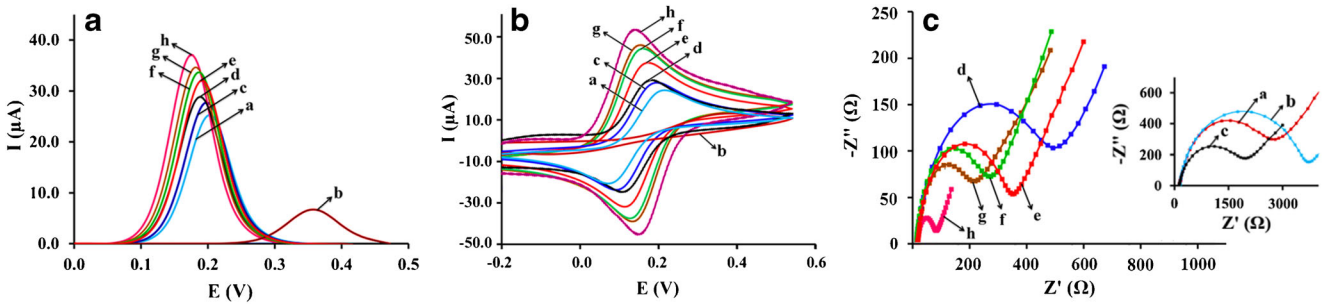

Fig. 2 **a** DPV, **b** CV, and **c** EIS curves of (a) unmodified GCE, and modified GCE with (b) GO, (c) ErGO, (d) SWCNT, (e) AuNP, (f) ErGO/AuNP, (g) SWCNT/AuNP, and (h) rGO-SWCNT/AuNP nanocomposites in a solution containing 3.0 mmol·L^{-1} $[Fe(CN)_6]^{3-}$/$[Fe(CN)_6]^{4-}$ (1:1) mixture and 0.1 mol·L^{-1} KCl

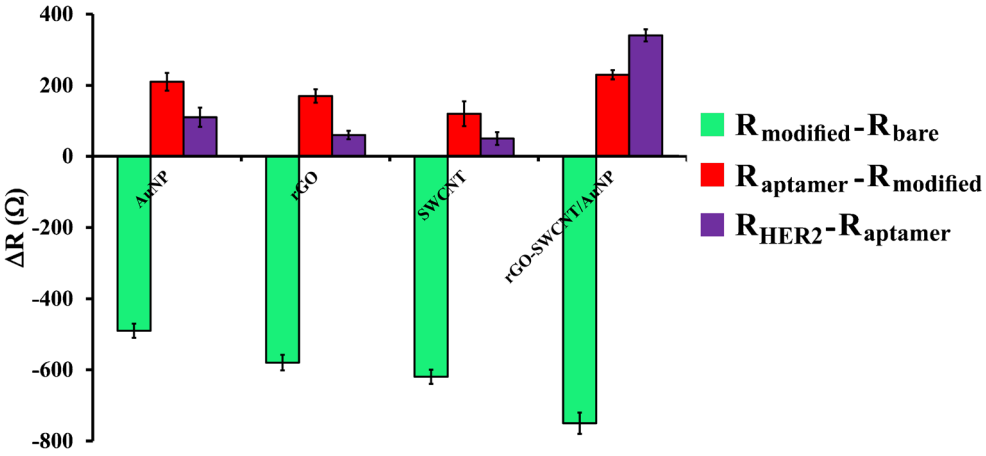

Fig. 3 Rct difference for each step in detection of HER2 was measured using presented method, in which AuNP, ErGO/AuNP, SWCNT/AuNP, and ErGO-SWCNT/AuNP were applied as sensitive layers. Nyquist plots were acquired in a solution containing 3.0 mmol·L^{-1} $[Fe(CN)_6]^{3-}$/$[Fe(CN)_6]^{4-}$ (1:1) mixture and 0.1 mol·L^{-1} KCl

and remaining oxygen-related defects of ErGO. Coating SWCNT/AuNP nanocomposite on GCE increases peak current (trace g) compared to SWCNT (trace d) which is due to high conductivity and good electron-transfer properties of AuNP. Modifying the electrodes with ErGO-SWCNT/AuNP, increases the current response more than GO, ErGO, SWCNT, AuNP, ErGO-SWCNT, SWCNT/AuNP, and ErGO/AuNP (trace h). This increase is the result of improved electron-transfer ability and unique benefits of SWCNT, ErGO, and AuNP and their synergy contributions.

Additionally, CV results (Fig. 2b) are similar to DPV results acquired under similar conditions. In the next step, EIS measurements were carried out using various nano-modified GCEs under similar conditions (Fig. 2c). The data was fitted well with an equivalent circuit (Fig. S-3). The results showed that in the case of ErGO-SWCNT/AuNP modified electrode, the amount of Rct is sharply reduced compared to bare and other modified electrodes because of the presence of SWCNT, ErGO, and AuNP in ErGO-SWCNT/AuNP. This might be due to great conductivity of SWCNT, ErGO, and AuNP.

Optimization of nanoprobe manufacturing process

In order to improve its performance and sensitivity, all parameters related to the electrochemical assay developed by ErGO-SWCNT/AuNP were optimized. Optimized parameters include the aptamer anti-HER2 concentration, aptamer immobilization time, and the interaction time between the HER2 and aptamer-confined electrode. The optimization results are presented in more detail in "Supplementary Materials" in more details (Section S2.3). The optimal concentration of aptamer, immobilization time, and interaction time are 200 nmol.L^{-1}, 9 h, and 40 min, respectively.

HER2 detection

EIS was used as a sensitive technique for the detection of HER2. Impedance of the electrode was determined in a solution containing 3.0 mmol·L^{-1} $[Fe(CN)_6]^{3-}$ /$[Fe(CN)_6]^{4-}$ (1:1) as redox probe and 0.1 mol·L^{-1} KCl. Immobilization of the aptamer on the nanomaterials modified GCE hinders the access of the redox probe to the electrode surface. This in turn results in low electron transfer efficiency and an increase of Rct in EIS measurements. After interaction of HER2 with aptamer-confined electrode, Rct increases again because more hindering of access of the redox couple to the electrode surface. The AuNP, SWCNT/AuNP, ErGO/AuNP, and ErGO-SWCNT/AuNP were used to prepare various types of HER2 assays. The quality of the immobilization of the APT and the sensitivity for the detection of the HER2 on the GCE modified

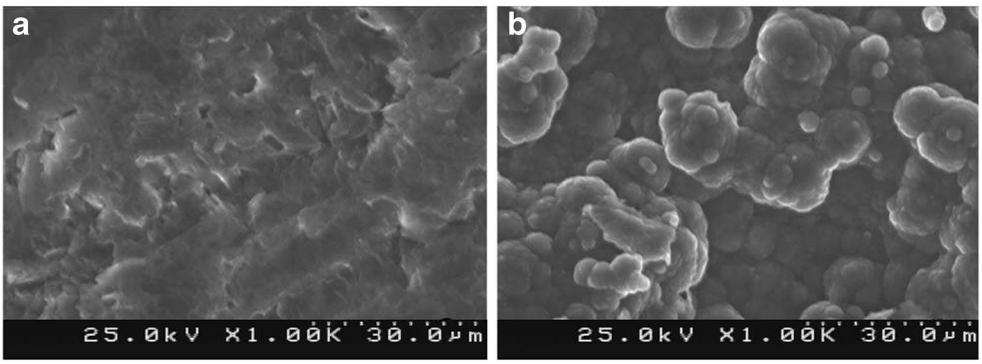

Fig. 4 SEM images of GCE/ErGO-SWCNT/AuNP/Apt: **a** before and **b** after bonding of HER2

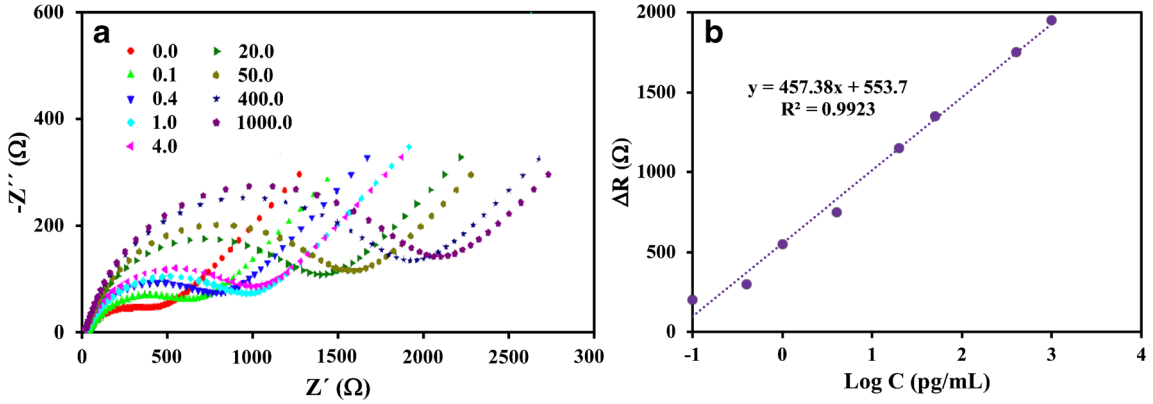

Fig. 5 **a** Nyquist plots of anti-HER2 nanoprobe for different concentrations of HER2 within 0 pg·mL^{-1} – 1000 pg·mL^{-1}, **b** Linear calibration plot for ΔRct vs. log C_{HER2}

with each of these nanocomposites were compared with each other. The EI spectrum of the different modified electrodes are shown in Fig. S-5 (A-D). Additionally, Fig. 3 shows changes in the Rct after modifying of the electrodes with nanomaterials (blue bar), aptamer (red bar) and after interaction of the aptamer with HER2 (green bar). The differences between Rct values (ΔR) were used as the main comparison criteria for before and after addition of a new nanocomposite layer.

For AuNP, SWCNT/AuNP, ErGO/AuNP, and ErGO-SWCNT/AuNP based nanoprobs, ΔR values after HER2 detection (C_{HER2} = 0.5 pg·mL^{-1}) are 108, 59, 52, and 340 Ω, respectively (Fig. 3). Values of ΔR show a significant signal after interaction of the aptamer-confined electrode with HER2 in the case of ErGO-SWCNT/AuNP modified electrode, compared to other nanomodified electrodes, making it the most appropriate electrode for HER2 detection. The SEM images of the aptamer functionalized GCE/ErGO-SWCNT/AuNP before and after interaction with HER2 is shown in the Fig. 4. by the SEM images. The images showed that, after the incubation of the nanoprobe in the HER2 solution, the protein captured by the aptamers could be observed on the surface of the electrode.

To obtain the calibration plot, several HER2 solutions in Tris buffer (pH = 7.4) were prepared with different concentrations and measured using ErGO-SWCNT/AuNP. Figure 5a shows the Nyquist plots of the aptamer modified GCE/ErGO-SWCNT/AuNP after binding with different concentrations of HER2 in Tris buffer. Results show that the Rct have increased with increase in the HER2 concentration. Figure 5b shows the calibration plot at various concentrations of HER2. As can be seen, logarithmic increase in HER2 concentration leads to linear increase in Rct. The calibration plot is linear in the range from 0.1 pg·L^{-1} to 1 ng·mL^{-1} with a detection limit of 0.05 pg·mL^{-1} at a signal-to-noise ratio of 3.

Selectivity

The competition with HER2 in the solution was also studied in order to evaluate the selectivity of the method. For this purpose, some proteins including lysozyme, BSA, human IgG, PSA, BHb, and thrombin were used. These proteins were also used to determine any probable non-specific adsorptions onto GCE/ErGO-SWCNT/AuNP/APT. To this end, the

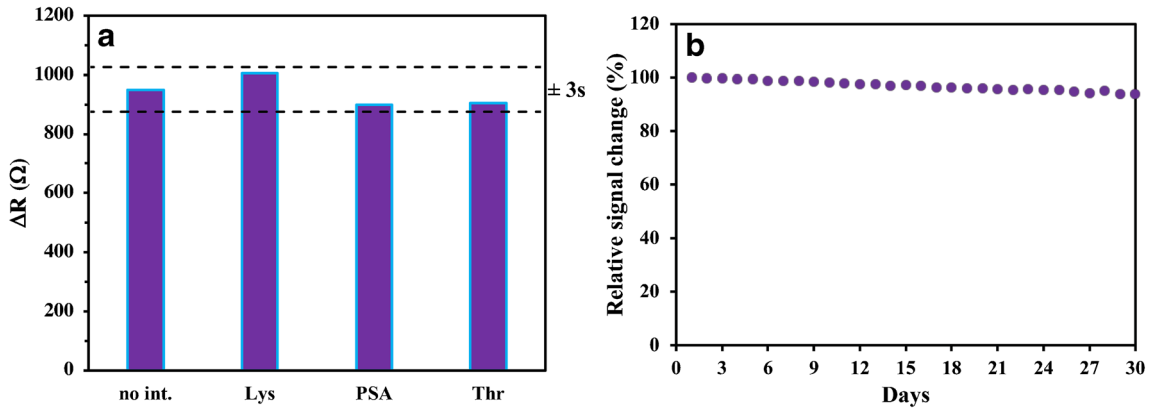

Fig. 6 (**a**) Effect of the presence of 100 pg·mL^{-1}, PSA, thrombin, and lysozyme on the EIS responses obtained with the GCE/rGO-SWCNT/AuNP/APT in competition with 10 pg·mL^{-1} HER2. (I) Time dependence of relative signal change corresponding to the original signal of the method at 10 pg·mL^{-1} HER2 on the first day of measurement

Table 1 Recovery measurements of HER2 spiked in serum samples from healthy persons

Sample no	Add ($pg{\cdot}mL^{-1}$)	Found ($pg{\cdot}mL^{-1}$)	Recovery (%)	RSD (%)
1	0	0.4	–	6.1
2	3	3.61	106.2	4.2
3	13	12.72	94.9	5.7
4	23	24.2	103.4	3.9
5	33	32.88	98.4	6.9

concentration of the HER2 was measured under optimal experimental conditions in the presence of these proteins. Figures 6a shows that after addition of PSA (100 $pg{\cdot}mL^{-1}$), thrombin (100 $pg{\cdot}mL^{-1}$), and lysozyme (100 $pg{\cdot}mL^{-1}$) to the solution containing HER2 (10 $pg{\cdot}mL^{-1}$), changes in Rct are not significant. This shows good selectivity of the method in the presence of other proteins. The results indicated that the GCE/ErGO-SWCNT/AuNP/APT only responds to HER2 and not to another proteins.

Reproducibility and storage stability

For the application of the method in the analysis of different real samples, it is necessary the method showed reproducible signals to HER2. Therefore, in order to measure reproducibility, ten electrodes (GCE/ErGO-SWCNT/AuNP/APT) were used for measuring 10 $pg{\cdot}mL^{-1}$ of HER2. The values of ΔR for the measurements of 10 $pg{\cdot}mL^{-1}$ HER2 have a Relative Standard Deviation (RSD) of 5.4%.

Storage stability of the GCE/ErGO-SWCNT/AuNP/APT might present an important issue during practical applications of HER2 detection. Time-dependency of current response, relative to the original signal for 10 pg mL^{-1} HER2 solution on the first day, is shown in Fig. 6b. Between measurements at different days, aptamer modified electrodes were kept at 4 °C under dry conditions. The results indicate that after 1 month, anti-HER2 nanoprobes signal for 10 $pg{\cdot}mL^{-1}$ HER2 solution is 94% of the original signal. This confirms excellent storage stability of GCE/ErGO-SWCNT/AuNP/APT.

Recovery test

In order to verify the accuracy of the method, the concentrations of HER2 in the spiked serum samples from normal human that diluted 400-fold were measured (Table 1). Using the standard addition method, the recoveries of HER2 detection in the spiked human serum samples are found in the range of 94.9%–106.2% ($n = 3$), representative the consistency and applicability of the GCE/ErGO-SWCNT/AuNP/APT for spiked sample analysis.

Serum sample testing

Finally, HER2 contents in six serum samples from breast cancer patients and ten serum samples from healthy persons were tested to determine the feasibility of GCE/ErGO-SWCNT/AuNP/APT for real sample analysis. To remove observational bias, each sample was analyzed in quintuple, and the resultant data are presented in Table S-1. As expected, the concentrations of HER2 in samples from cancer patients are higher than those for healthy subjects, which is consistent with the previous reports. Therefore, this method can be used to differentiate healthy people from people with breast cancer, and even measuring the amount of HER2 in the serum samples to assess the

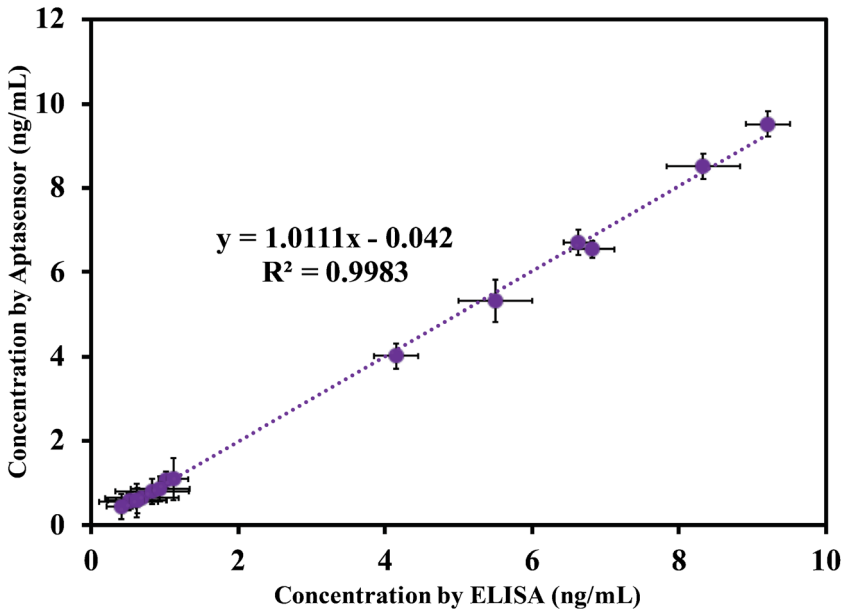

Fig. 7 Regression analysis of the detection of HER2 with ELISA in human serum samples

prognosis of the cancer. Besides, in order to verify the reliability of the aptamer-based assay, the serum samples were also analyzed by commercial ELISA kit. As listed in Table S-1, the HER2 levels determined by our method were in good agreement with ELISA results. The results of the two methods were analyzed by linear regression, which gave a R^2 of 99.83 (Fig. 7). The results show that the method has advantages such as high sensitivity, accuracy and specificity for detection of HER2 in serum samples.

Conclusions

We introduce a novel electrochemical aptamer-based assay based on ErGO-SWCNT/AuNP nanocomposite for detection of HER2 protein. In the presence of HER2, aptamer on the surface of the GCE modified with ErGO-SWCNT/AuNP adsorbs the target HER2 molecules. This creates an electron barrier and restricts electron transfer which results in increase of Rct in EIS. The results indicate that the amount of immobilized aptamer molecules on the GCE surface increases after modification using ErGO-SWCNT/AuNP. Method of using the nanocomposite in electrochemical assays proposed in the current study can also be applied for detection of other molecules and proteins. This means that the current aptamer-based approach can be a powerful and selective tool for developing and improving novel electrochemical assays.

Acknowledgements The authors gratefully acknowledge the support of this work by the Research Council of Vali-e-Asr University of Rafsanjan (VRU), Iran.

Compliance with ethical standards The author(s) declare that they have no competing interests.

References

1. Hurvitz S, McCann K (2019) HER2-positive breast cancer. Elsevier, St. Louis
2. Hung M-C, Matin A, Zhang Y, Xing X, Sorgi F, Huang L, Yu D (1995) HER-2/neu-targeting gene therapy-a review. Gene 159:65–71
3. Perez EA, Cortés J, Gonzalez-Angulo AM, Bartlett JMS (2014) HER2 testing: current status and future directions. Cancer Treat Rev 40:276–284
4. Xu B, Shen J, Guo W, Zhao W, Zhuang Y, Wang L (2019) Impact of the 2018 ASCO/CAP HER2 guidelines update for HER2 testing by FISH in breast cancer. Pathol Res Pract 215:251–255
5. Hirschmann A, Lamb TA, Marchal G, Padilla M, Diebold J (2012) Simultaneous analysis of HER2 gene and protein on a single slide facilitates HER2 testing of breast and gastric carcinomas. Am J Clin Pathol 138:837–844
6. Lim S-J, Cantillep A, Carpenter PM (2013) Validation and workflow optimization of human epidermal growth factor receptor 2 testing using INFORM HER2 dual-color in situ hybridization. Hum Pathol 44:2590–2596
7. Ding J, Zhou Y, Li JJ, Jiang LP, He ZW, Zhu JJ (2015) Screening of HER2 overexpressed breast cancer subtype in vivo by the validation of high-performance long-term, and noninvasive fluorescence tracer. Anal Chem 87:12290–12297
8. Kao KJ, Tai CH, Chang WH, Yeh TS, Chen TC, Lee GB (2015) A fluorescence in situ hybridization (FISH) microfluidic platform for detection of HER2 amplification in cancer cells. Biosens Bioelectron 69:272–279
9. Zhang M, Gao G, Ding Y, Deng C, Xiang J, Wu H (2019) A fluorescent aptasensor for the femtomolar detection of epidermal growth factor receptor-2 based on the proximity of G-rich sequences to Ag nanoclusters. Talanta 199:238–243
10. Shen C, Zeng K, Luo J, Li X, Yang M, Rasooly A (2017) Self-assembled DNA generated electric current biosensor for HER2 analysis. Anal Chem 89:10264–10269
11. Qureshi A, Gurbuz Y, Niazi JH (2015) Label-free capacitance based aptasensor platform for the detection of HER2/ErbB2 cancer biomarker in serum. Sensors Actuators B 220:1145–1151
12. Shen C, Liu S, Li X, Zhao D, Yang M (2018) Immunoelectrochemical detection of the human epidermal growth factor receptor 2 (HER2) via gold nanoparticle-based rolling circle amplification. Microchim Acta 185:547–553
13. Chai Y, Li X, Yang M (2019) Aptamer based determination of the cancer biomarker HER2 by using phosphate-functionalized MnO2 nanosheets as the electrochemical probe. Microchim Acta 186:316–322
14. Marques RCB, Viswanathan S, Nouws HPA, Delerue-Matos C, González-García MB (2014) Electrochemical immunosensor for the analysis of the breast cancer biomarker HER2 ECD. Talanta 129:594–599
15. Bahadır EB, Sezgintürk MK (2015) Applications of electrochemical immunosensors for early clinical diagnostics. Talanta 132:162–174
16. Pacheco JG, Rebelo P, Freitas M, Nouws HPA, Delerue-Matos C (2018) Breast cancer biomarker (HER2-ECD) detection using a molecularly imprinted electrochemical sensor. Sensors Actuators B 273:1008–1014
17. Sharma S, Zapatero-Rodríguez J, Saxena R, O'Kennedy R, Srivastava S (2018) Ultrasensitive direct impedimetric immunosensor for detection of serum HER2. Biosens Bioelectron 106:78–85
18. Marques RCB, Costa-Rama E, Viswanathan S, Nouws HPA, Costa-García A, Delerue-Matos C, González-García MB (2018) Voltammetric immunosensor for the simultaneous analysis of the breast cancer biomarkers CA 15-3 and HER2-ECD. Sensors Actuators B 255:918–925
19. Heydari-Bafrooei E, Askari S (2017) Ultrasensitive aptasensing of lysozyme by exploiting the synergistic effect of gold nanoparticle-modified reduced graphene oxide and MWCNTs in a chitosan matrix. Microchim Acta 184:3405–3413
20. Ensafi AA, Jamei HR, Heydari-Bafrooei E, Rezaei B (2016) Electrochemical study of quinone redox cycling: a novel application of DNA-based biosensors for monitoring biochemical reactions. Bioelectrochemistry 111:15–22
21. Yang S, You M, Zhang F, Wang Q, He P (2018) A sensitive electrochemical aptasensing platform based on exonuclease recycling amplification and host-guest recognition for detection of breast cancer biomarker HER2. Sensors Actuators B 258:796–802
22. Yang Y, Yang X, Yang Y, Yuan Q (2018) Aptamer-functionalized carbon nanomaterials electrochemical sensors for detecting cancer relevant biomolecules. Carbon 129:380–395
23. Gupta S, Murthy CN, Prabha CR (2018) Recent advances in carbon nanotube based electrochemical biosensors. Int J Biol Macromol 108:687–703
24. Arkan E, Saber R, Karimi Z, Shamsipur M (2015) A novel antibody–antigen based impedimetric immunosensor for low level detection of HER2 in serum samples of breast cancer patients via

modification of a gold nanoparticles decorated multiwall carbon nanotube-ionic liquid electrode. Anal Chim Acta 874:66–74

25. Tabasi A, Noorbakhsh A, Sharifi E (2017) Reduced graphene oxide-chitosan-aptamer interface as new platform for ultrasensitive detection of human epidermal growth factor receptor 2. Biosens Bioelectron 95:117–123
26. Yan H, Tang X, Zhu X, Zeng Y, Lua X, Yin Z, Lu Y, Yang Y, Li L (2018) Sandwich-type electrochemical immunosensor for highly sensitive determination of cardiac troponin I using carboxyl-terminated ionic liquid and helical carbon nanotube composite as platform and ferrocenecarboxylic acid as signal label. Sensors Actuators B 277:234–240
27. Scheller FW, Zhang X, Yarman A, Wollenberger U, Gyurcsányi RE (2019) Molecularly imprinted polymer-based electrochemical sensors for biopolymers. Curr Opin Electrochem 14:53–59
28. Labib M, Green B, Mohamadi RM, Mepham A, Ahmed SU, Mahmoudian L, Chang I-H, Sargent EH, Kelley SO (2016) Aptamer- and antisense-mediated two-dimensional isolation of specific cancer cell subpopulations. J Am Chem Soc 1388:2476–2479
29. Zhang Z, Chen HH, Xing CY, Guo MY, Xu FG, Wang XD, Gruber HJ, Zhang BL, Tang JL (2011) Sodium citrate: a universal reducing agent for reduction / decoration of graphene oxide with au nanoparticles. Nano Res 4:599–611
30. Sharma H, Kaushik V, Avasthi DK, Shukla AK, Vankar VD (2012) Au-nanoparticles-decorated MWCNTs demonstrating enhanced fluorescence and Raman spectroscopy. AIP Conf Proc 1451:58–60